THE JOURNAL OF BIOLOGICAL CHEMISTRY VOL. 291, NO. 6, pp. 2602–2615, February 5, 2016

Characterization of a Novel Intestinal Glycerol-3-phosphate Acyltransferase Pathway and Its Role in Lipid Homeostasis*

Received for publication, August 6, 2015, and in revised form, December 3, 2015 Published, JBC Papers in Press, December 7, 2015, DOI 10.1074/jbc.M115.683359

Irani Khatun[‡], Ronald W. Clark[‡], Nicholas B. Vera[‡], Kou Kou[‡], Derek M. Erion[‡], Timothy Coskran[§], Walter F. Bobrowski[§], Carlin Okerberg[§], and Bryan Goodwin[‡1]

From the [‡]Cardiovascular and Metabolic Diseases Research Unit, Pfizer Worldwide Research and Development, Cambridge, Massachusetts 02139 and [§]Drug Safety Research and Development, Pfizer Worldwide Research and Development, Groton, Connecticut 06340

Dietary triglycerides (TG) are absorbed by the enterocytes of the small intestine after luminal hydrolysis into monacylglycerol and fatty acids. Before secretion on chylomicrons, these lipids are reesterified into TG, primarily through the monoacylglycerol pathway. However, targeted deletion of the primary murine monoacylglycerol acyltransferase does not quantitatively affect lipid absorption, suggesting the existence of alternative pathways. Therefore, we investigated the role of the glycerol 3-phosphate pathway in dietary lipid absorption. The expression of glycerol-3-phosphate acyltransferase (GPAT3) was examined throughout the small intestine. To evaluate the role for GPAT3 in lipid absorption, mice harboring a disrupted GPAT3 gene (*Gpat3*$^{-/-}$) were subjected to an oral lipid challenge and fed a Western-type diet to characterize the role in lipid and cholesterol homeostasis. Additional mechanistic studies were performed in primary enterocytes. GPAT3 was abundantly expressed in the apical surface of enterocytes in the small intestine. After an oral lipid bolus, *Gpat3*$^{-/-}$ mice exhibited attenuated plasma TG excursion and accumulated lipid in the enterocytes. Electron microscopy studies revealed a lack of lipids in the lamina propria and intercellular space in *Gpat3*$^{-/-}$ mice. *Gpat3*$^{-/-}$ enterocytes displayed a compensatory increase in the synthesis of phospholipid and cholesteryl ester. When fed a Western-type diet, hepatic TG and cholesteryl ester accumulation was significantly higher in *Gpat3*$^{-/-}$ mice compared with the wild-type mice accompanied by elevated levels of alanine aminotransferase, a marker of liver injury. Dysregulation of bile acid metabolism was also evident in *Gpat3*-null mice. These studies identify GPAT3 as a novel enzyme involved in intestinal lipid metabolism.

The ability of an organism to efficiently extract energy-rich nutrients from its diet is critical for survival. Triglycerides (TG)[2] are energy-dense lipid molecules; however, their biophysical properties preclude direct absorption in the gut. The primary site for the absorption of TG and other dietary lipids is the small intestine. Lipid absorption is a multistep process that begins with the intraluminal emulsification of fat by bile acids, which in turn facilitates hydrolysis by multiple lipases. TG hydrolysis leads to the liberation of monoacylglycerol (MAG) and free fatty acid (FFA). Absorption of these hydrolyzed products occurs in the epithelial monolayer lining the villi and involves both passive diffusion and facilitated transport. After absorption, FFAs are primarily reesterified into TG and either temporarily stored as cytosolic lipid droplets (CLDs) or packaged into chylomicrons and secreted into the lymphatic vessels of the lamina propria through the basolateral surface of enterocytes (1).

There are two primary routes for TG synthesis, namely, the MAG and glycerol 3-phosphate (G3P) pathways. Both pathways produce diacylglycerol (DAG) as a common intermediate. In the MAG pathway DAG is directly synthesized from *sn*-2 MAG through the action of monoacylglycerol acyltransferases (MGAT). In the G3P pathway DAG is produced by three reactions. Initially, G3P is acylated by the members of the glycerol-3-phosphate acyltransferase (GPAT) family. The resultant lysophosphatidic acid is further acylated by 1-acylglycerol-3-phosphate *O*-acyltransferases and then dephosphorylated by phosphatidic acid phosphatase enzymes to produce DAG. In most cell types producing TG, the G3P pathway is the primary route for TG synthesis (2). In the intestine MAG is the preferred acceptor of FFAs, and the MAG pathway accounts for ~80% of TG synthesis (3–7). Importantly, targeted disruption of the murine *Mogat2* gene, which encodes the predominant MGAT in the small intestine, does not quantitatively affect lipid absorption. Rather, loss of MGAT2 activity in the gut results in a shift in the spatiotemporal profile of lipid absorption with the distal small intestine assuming a more prominent role in this process (8). Although the enzymes responsible for TG absorption in *Mogat2*$^{-/-}$ mice have not been delineated, it is possible that a hitherto unidentified MGAT compensates for the loss of MGAT2 or that the MAG is further hydrolyzed to glycerol and FFA and enters the G3P pathway (9–11).

To date, four mammalian GPAT genes (GPAT1–4) have been identified. GPATs catalyze the first committed step in TG

* The authors declare that they have no conflict of interest with the content of this article.

[1] To whom correspondence should be addressed: Pfizer Worldwide Research and Development, Cardiovascular and Metabolic Diseases Research Unit, 610 Main St., Cambridge, MA 02139. Tel.: 617-874-0182; E-mail: bryan.goodwin@pfizer.com.

[2] The abbreviations used are: TG, triglyceride; GPAT, glycerol-3-phosphate acyltransferase; G3P, glycerol 3-phosphate; FFA, free fatty acid; CLD, cytosolic lipid droplet; DAG, diacylglycerol; MAG, monoacylglycerol: MGAT, monoacylglycerol acyltransferase; DGAT, diacylglycerol acyltransferase; CE, cholesteryl ester; WTD, Western-type diet; UPLC, ultraperformance liquid chromatography; GIP, gastric inhibitory polypeptide; GLP-1, glucagon-like peptide-1; CPT1A, carnitine palmitoyltransferase 1a; Sf, floatation coefficient; CM, chylomicron; TBA, total bile acid; NEM, *N*-ethylmaleimide.

synthesis (12). GPAT enzymes are broadly categorized based on their sensitivity to inhibition by sulfhydryl group-modifying reagents like *N*-ethylmaleimide (NEM) and subcellular location. Thus, GPAT1 and GPAT2 localize to mitochondria, whereas GPAT3 and GPAT4 are nominally microsomal. GPAT1 is resistant to inhibition by NEM, whereas GPAT2, -3, and -4 are NEM-sensitive (13–17). In mice, the gene encoding GPAT4 is highly expressed in the liver, whereas GPAT3 is predominantly expressed in the small intestine and adipose tissue (18). *Gpat3*$^{-/-}$ mice have reduced NEM-sensitive GPAT activity in white adipose depots and liver and, when maintained on standard chow, do not exhibit any obvious metabolic abnormalities aside from increased hepatic cholesterol and cholesteryl ester levels. When fed a high fat diet, modest metabolic perturbations, including decreased body weight gain and elevated physical activity, were evident in female mice (18). Given the abundant expression of GPAT3 in the small intestine, we investigated a potential role for this enzyme in intestinal lipid absorption. We observed a distinct regional localization for GPAT3 protein to the jejunum, the primary site for lipid absorption. We demonstrate for the first time that GPAT3 plays a role in intestinal lipid absorption and that loss of GPAT3 expression results in abnormalities in dietary lipid absorption and a disruption of enteric and hepatic lipid homeostasis.

Experimental Procedures

Animal Studies—GPAT3 knock-out (*Gpat3*$^{-/-}$) mice were generated as described previously (18). Animals were bred at Taconic (Germantown, NY) and transferred to a Pfizer facility at least 14–21 days before the start of experiments. Mice were housed under standard laboratory conditions on a 12-h light, 12-h dark cycle (lights on at 06:00 a.m.) and allowed free access to food and water. All studies were performed according to Pfizer internal animal use protocols and approved by Pfizer's Institutional Animal Care and Use Committee. All studies used age-matched (14–16 weeks) male wild-type and *Gpat3*$^{-/-}$ mice. For studies using fed and fasted cohorts, mice were either allowed standard laboratory rodent chow 5001 *ad libitum* or fasted for 6 h from 06:00 a.m. to 12:00 p.m. In high fat diet feeding studies wild-type and *Gpat3*$^{-/-}$ mice were maintained on standard laboratory rodent chow (5001) or fed a Western-type diet (WTD, TD88137, Harlan Teklad, 42% kcal from fat, 0.2% cholesterol, w/w) for 4 weeks.

In Vivo Flux and Dietary Fat Uptake Studies—For *in vivo* flux studies mice maintained on standard laboratory chow *ad libitum* were fasted for 6 h, injected non-ionic detergent poloxamer 407 (intraperitoneally) (19), and 30 min later administered an oral intragastric bolus of olive oil (15 ml/kg, *per os*) (20, 21) containing [^{3}H]triolein (0.5 μCi/g) 30 min later. Plasma was collected by tail vein bleeds before the oral gavage after P407 administration and 30, 60, 90, and 120 min post dose to determine rate of postprandial TG secretion. FPLC was performed on plasma collected 2 h post-dose by cardiac stick to isolate different lipoprotein population to determine triglyceride mass and tracer incorporation. To assess distribution of dietary lipids in the tissue, small intestines were flushed with 0.5 mM sodium taurocholate in PBS and cut into 2.5-cm sections. The segments were weighed and digested in 500 μl of 1 N NaOH overnight and mixed with liquid scintillation mixture to measure counts per mg of segments by scintillation counter.

Western Immunoblotting—Microsomes were isolated as described elsewhere (22). Briefly, intestinal segments were homogenized in buffer containing 250 mM sucrose, 20 mM Tris-HCl, pH 7.4, 1 mM EDTA. Cellular debris was removed by centrifugation at 500 $\times$ *g* for 10 min, and crude mitochondrial pellets were obtained by centrifugation of the 500 $\times$ *g* supernatant at 15,000 $\times$ *g* for 10 min. The supernatant was centrifuged at 106,000 $\times$ *g* for 1 h, and the resultant pellet, corresponding to the microsomal fraction, was resuspended in 20 mM Tris-HCl, 0.5 M NaCl (pH 7.4), lysed, and centrifuged at 106,000 $\times$ *g* for 1 h to obtain the luminal contents. Protease inhibitor mixture (Sigma) was included in all of the solutions used in this isolation procedure. Proteins (50 μg) were separated on 4–20% Novex Tris-glycine gels (Life Technologies), transferred onto 0.45-μm nitrocellulose, and developed for GPAT3 expression using (LPAAT-θ), T-17 (Santa Cruz Biotechnology, Dallas, TX), and secondary antibody, anti-goat IgG, horseradish peroxidase conjugate (Promega, Sunnyvale, CA).

GPAT and MGAT Activity Assays—GPAT activity assays in the murine small intestinal segments were performed ostensibly as described elsewhere (17, 18, 23). Intestinal mucosal tissues were scraped and homogenized in ice-cold PBS, and enzyme reactions were initiated by the addition of 6 μg of microsomal protein in 75 mM Tris-HCl (pH 7.5), 4 mM $MgCl_2$, 1 mg/ml fatty acid free BSA, 150 μM [^{14}C]glycerol 3-phosphate (55 mCi/mmol) and 50 μM oleoyl-CoA. Samples were incubated with the buffer and the substrate for 15 min at room temperature. For NEM-resistant activity, the total cell lysates were preincubated with 0.4 mM NEM for 15 min on ice before the initiation of the GPAT reaction. Products were extracted using chloroform and methanol and separated by thin-layer chromatography (TLC) using chloroform:methanol:water (65:25:4), bands were scraped, and ^{14}C counts were quantitated using scintillation counter. MGAT activity assays in the intestinal mucosal tissue were determined by measuring incorporation of the [^{14}C]oleoyl moiety into diacylglycerol. Reactions were initiated by incubating microsomal proteins with 4 μM [^{14}C]decanoyl-CoA (PerkinElmer Life Sciences) in the presence or absence (control) of 35 μM 2-oleoylglycerol in 50 mM HEPES (pH 7.4), 10 mM $MgCl_2$, 0.001% Triton X-100, and 2.5% v/v acetone. A non-selective lipase inhibitor MAFP (methyl arachidonyl fluorophosphates) was added to block the hydrolysis of both product and substrate as previously described (24). After 30 min reactions were terminated by adding 50 μl of 1% phosphoric acid. Lipids were extracted using $CHCl_3$/methanol (2:1, v/v) and separated by TLC, and DAG bands were quantified.

Immunohistology, Immunohistochemistry, and Electron Microscopy—The entire small intestine was removed for histological analysis and cut into ~5.0-cm segments and flushed with physiological saline. From each 5.0-cm segment cross-sections were fixed with 10% neutral-buffered formalin and processed to paraffin blocks. Individual small intestine segments or liver tissues were embedded in paraffin blocks so that areas of could be evaluated on one slide per animal. Five-micron sections were cut using a rotary microtome and mounted on slides for routine

hematoxylin and eosin (H&E) staining and immunohistochemistry. For Brightfield immunohistochemistry, 5-μm sections were deparaffinized, hydrated, and treated with Biogenex Citra (Biogenex, Fremont, CA) using the Decloaking Chamber (Biocare Medical, Concord, CA) to expose the antigenic sites. Endogenous peroxidase was blocked by incubations with 3.0% solution of hydrogen peroxide (ThermoFisher, Waltham, MA) for 10 min, and nonspecific sites were blocked using Dako serum-free protein block (Dako, Carpinteria, CA) for 20 min. The following antibodies were all incubated for 60 min at room temperature: goat anti-GPAT3 1:2000 (Santa Cruz Biotechnology, Dallas, TX) and guinea pig anti-TIP47 1:2000 (Progen, Heidelberg, Germany). GPAT3 was detected using Biocare goat probe horseradish peroxidase followed by visualization with Dako Liquid diaminobenzidine (DAB+). All slides were counterstained with Mayer's hematoxylin (Dako) and mounted using permanent mounting medium (Sakura, Torrance, CA). For immunofluorescence immunohistochemistry, 5-μm sections were prepared as described above. Goat anti-GPAT3 and guinea pig anti-TIP47 were used at a dilution of 1:500 for 60 min at room temperature. Detection was accomplished using Alexa fluor secondary antibodies, donkey anti-goat IgG Alexa 488, and donkey anti-guinea pig IgG Alexa 594 secondary antibodies (Life Technologies) for 45 min at room temperature. All slides were mounted with Prolong Gold plus DAPI (Life Technologies). For electron microscopy, ~1 mm of jejunum was fixed in 0.1 M phosphate-buffered fixative containing 4% formaldehyde (methanol-free) and 1% glutaraldehyde for a minimum of 24 h. Samples were rinsed in 0.1 M phosphate buffer and post-fixed in 0.1 M phosphate-buffered 1% osmium tetraoxide for 2 h. Samples were rinsed thoroughly and dehydrated through graded ethanol and embedded in epoxy resin. Sections (~1.5 μm) were stained with 1% paraphenylenediamine in 100% methanol for 10 min followed by 2 rinses in 100% ethanol for total of 5 min and dried, and coverslips were placed on top before electron microscopy. Selected tissue blocks were trimmed to regions of interest, and sections were prepared (~90 nm thin) and were prepared with an ultracut UCT ultramicrotome (Leica). The sections were stained with uranyl acetate and lead citrate and examined using a Hitachi H-7100 transmission EM, and representative images were digitally captured (advanced microscopy techniques).

Liquid Chromatography-Mass Spectrometry Analysis (LC-MS)—Lipomic analysis of small intestine and liver was performed using LC-MS. Tissues were weighed and homogenized in methanol:water (1:1 v/v) using a Qiagen TissueLyzer (Qiagen, Germantown, MD). FFAs were extracted using methanol: water (80:20 v/v) and heptadecanoic acid (200 nM) as an internal standard and analyzed by ultra performance liquid chromatography (UPLC)-MS using a Waters Acquity UPLC coupled to a Thermo LTQ Orbitrap Velos mass spectrometer. FFA species were separated by reversed-phase chromatography on a Waters Acquity UPLC BEH C18 column, 1.7 μm, 2.1 × 50 mm and analyzed on the mass spectrometer using negative ion electrospray ionization in the full scan MS mode. FFA identification and LC chromatogram peak integration was performed with Thermo Sieve software. For acylcarnitines, tissues were homogenized as described above, and long chain acylcarnitines were extracted with dichloromethane:isopropyl alcohol:methanol (25:10:65, v/v/v) containing palmitoyl-L-carnitine (*N*-methyl-d_3) hydrochloride (200 nM) as the internal standard. Short chain acylcarnitines were extracted with methanol:water (3:1 v/v) containing 200 nM acetyl-L-carnitine (*N*-methyl-d_3) hydrochloride as the internal standard. Acylcarnitine extracts were then analyzed by UPLC-MS/MS using a Waters Acquity UPLC coupled to an AB Sciex QTRAP 5500 mass spectrometer. Long chain acylcarnitine species were separated by reversed phase chromatography on a Waters Acquity UPLC BEH300 C4 column, 1.7 μm, 2.1 × 50 mm. Short chain acylcarnitine species were separated by hydrophilic interaction liquid chromatography (HILIC) on a Waters Acquity UPLC BEH HILIC column, 1.7 μm, 2.1 × 150 mm. Acylcarnitines were then analyzed on the mass spectrometer using positive ion electrospray ionization in the multiple reaction monitoring (MRM) mode. LC chromatogram peak integration was performed with AB Sciex MultiQuant software. All data reduction was performed with in-house software.

Primary Enterocyte Isolation and ex Vivo Tracer Studies—Murine primary enterocytes were isolated using EDTA treatment as described elsewhere (25–27). Luminal contents were collected at the final wash step and centrifuged at 1500 rpm for 5 min at room temperature, and pellets were resuspended in DMEM containing 95% O_2 and 5% CO_2. Cellular uptake and secretion assays were performed as previously described (26, 27). Briefly, isolated enterocytes were incubated with 0.5 μCi/ml [^{3}H]oleic acid/[^{14}C]cholesterol (PerkinElmer Life Sciences) for 1 h at 37 °C with constant shaking, and cell suspensions were gassed with 95% O_2 and 5% CO_2 at 15-min intervals. Cell suspensions were centrifuged at 1500 rpm for 5 min, the supernatant was discarded, and pellets were washed with oxygenated DMEM three times. Cell pellets were lysed (250 mM sucrose, 20 mM Tris-HCl (pH 7.4), 1 mM EDTA), and an aliquot was used for protein determination to normalize the counts with the protein. Lipids were extracted from the remaining cell lysate using modified a Bligh and Dyer method in a 2:1 ratio of methanol:chloroform. Total lipid counts were determined on an aliquot of the extract by liquid scintillation, and incorporation of radioisotope into different intracellular lipids was monitored by TLC separation.

For secretion studies, primary enterocytes were isolated and incubated with 0.5 μCi/ml of [^{3}H]oleic acid or [^{14}C]cholesterol for 1 h, and cell pellets were collected and washed as described above after incubation. Cells were resuspended in modified DMEM (27). Media were collected after 2 h, and lipids were extracted to measure total counts and separated on TLC. For cholesterol secretion, media were further subjected to density gradient ultracentrifugation, and counts were measured (26, 27).

High performance Liquid Chromatography (HPLC), Tissue Lipid and Bile Acid Analysis—Liver or intestinal tissues were weighed, and lipids were extracted using a modified Bligh and Dyer method. Before lipid determination, the intestine was thoroughly flushed with saline to ensure no contamination with residual luminal lipids. Phospholipid C, triglycerides M, and total and free cholesterol assays were purchased from Wako (Richmond, VA). HPLC of frozen liver samples to determine

hepatic lipid levels was performed exactly as described previously (18). For determination of hepatic bile acid levels, liver samples were homogenized in 75% ethanol and incubated at 50 °C in a water bath. Samples were briefly spun, and supernatant containing bile acids was collected. Bile acid concentrations were determined using a commercially available kit (Diazyme, Poway, CA).

Plasma Clinical Chemistry and Incretin Analysis—Plasma analytes were analyzed using clinical analyzer, Hitachi Cobas (Hoffmann-La Roche). Plasma total glucagon-like peptide-1 (GLP-1) and gastric inhibitory polypeptide (GIPO were determined using commercial assays (EMD Millipore, Darmstadt, Germany).

RNA Isolation and Gene Expression—Tissue-specific expression of the *Gpat3* gene was determined on RNA obtained from Clontech (Mountain View, CA). For all other gene expression assays, RNA was extracted from aliquots of instantly frozen tissue samples using Qiazol according to the manufacturer's instructions (Qiagen, Germantown, MD). Gene expression was analyzed using real-time PCR system. All primer-probe assays were from Life Technologies with assay numbers as follows: DGAT1 (diacylglycerol *O*-acyltransferase 1), Mm00515643_m1; DGAT2 (diacylglycerol *O*-acyltransferase 2), Mm00499536_m1; MGAT2 (monoacylglycerol *O*-acyltransferase 2), Mm00624192_m1; CPT1A (carnitine palmitoyltransferase 1a, liver), Mm01231183_m1; ACADL (acyl-coenzyme A dehydrogenase, long-chain), Mm00599660_m1; ACADM (acyl-coenzyme A dehydrogenase, medium chain), Mm01323360_g1; ACAA2 (acetyl-coenzyme A acyltransferase 2), Mm00624282_m1; ACOT1 (acyl-CoA thioesterase 1), Mm01622471_s1; ACOT2 (acyl-CoA thioesterase 2) Mm01622461_s1; ACAA (acetyl-coenzyme A acyltransferase 1B), Mm00728805_s1; ACOX1 (acyl-coenzyme A oxidase 1, palmitoyl), Mm01246834_m1; SCARB1 (scavenger receptor class B, member 1), Mm00450234_m1; FGF15 (fibroblast growth factor 15), Mm00433278_m1; SHP (nuclear receptor subfamily 0, group B, member 2), Mm00442278_m1; PPARA (peroxisome proliferator-activated receptor α), Mm00440939_m1; FXR (NR1H4, nuclear receptor subfamily 1, group H, member 4), Mm00436425_m1; APOA4 (apolipoprotein A-IV), Mm00431814_m1; GCG (glucagon), Mm00801714_m1; GIP, Mm00433601_m1; PPIA (peptidylprolyl isomerase A), Mm02342430_g1; GPAT3 (1-acylglycerol-3-phosphate *O*-acyltransferase 9), Mm04211965_m1; GPAT4 (1-acylglycerol-3-phosphate *O*-acyltransferase 6 (lysophosphatidic acid acyltransferase, ζ)), Mm00497622_m1.

Statistical Analysis—Statistical tests were performed (GraphPad Prism software, version 6.0, GraphPad, La Jolla, CA).

Results

GPAT3 Was Abundantly Expressed in the Absorptive Epithelial Cells of the Small Intestine—Previous studies have documented a role for GPAT3 in the synthesis of triacylglycerol in adipocytes (17, 18, 28, 29). To further investigate the physiological role of GPAT3, the level of GPAT3 mRNA was determined in a panel of tissues. In line with previous reports, the murine *Gpat3* gene was abundantly expressed in the adipose, heart, and small intestine (Fig. 1*A*). GPAT3 protein was detectable in microsomes isolated from the jejunum. A distribution profile of GPAT3 along the small intestine exhibited expression confined to the central (jejunal) portion of the small intestine that was strongly induced after a 6-h fast (Fig. 1*B*). As expected, immunoreactive GPAT3 was absent in *Gpat3*$^{-/-}$ mice (Fig. 1*B*). Activity assays demonstrated an ~40% decrease in total GPAT activity in the *Gpat3*$^{-/-}$ jejunum (6.44 ± 0.35 and 4.05 ± 0.45 nmol/min/mg in wild-type and *Gpat3*$^{-/-}$, respectively) mice. The decrease in jejunal total GPAT activity was primarily attributable to a reduction in NEM-sensitive activity. No significant changes were observed in jejunal NEM-resistant activity as well as total and NEM-sensitive GPAT activities in the duodenum and ileum of wild-type and *Gpat3*$^{-/-}$ mice (Fig. 1*C*). Taken together these data indicate that GPAT3 is abundantly expressed in the jejunal region of the mouse small intestine.

Immunohistochemistry further localized GPAT3 to the absorptive epithelium of the villus (Fig. 2*A*). Immunoreactive staining was completely absent in *Gpat3*$^{-/-}$ mice. During lipid absorption, enterocytes transiently store TGs in CLD before packaging and secretion in chylomicron particles (30). To determine if GPAT3 localizes to lipid droplets during the absorptive period, wild-type and *Gpat3*$^{-/-}$ mice were administered an oral bolus of olive oil after a 6-h fast. GPAT3 was exclusively expressed on the apical region of the wild-type enterocytes (Fig. 2*B*, *left panel*). We further monitored location of the PAT (perilipin) family protein TIP47 (PLIN3), which has been reported to be highly expressed in the enterocytes and localizes to CLD after acute high fat feeding (30, 31). In similarity to GPAT3, TIP47 was readily detectable in the apical region of the enterocytes with dense staining around the surface of the lipid droplets (Fig. 2*B*, *right panel*). In these lipid-laden villi, intense TIP47 staining was evident on the surface of the lipid droplet, but although we could identify GPAT3 immunofluorescence in the proximity to lipid droplets (*inset*, *left panel*, Fig. 2*C*). it was not possible to definitively colocalize GPAT3 and TIP47 to CLD Fig. 2*C*, *left panel*). The pattern of TIP47 staining did change in GPAT3-null enterocytes (Fig. 2*C*, *right panel*). These data demonstrate that GPAT3 and TIP47 localize to the apical surface of the enterocyte.

Gpat3$^{-/-}$ *Mice Exhibited Dysregulated Intestinal Lipid Absorption*—Given the abundant expression of GPAT3 in the small intestine, we next examined whether loss of GPAT3 function modulated intestinal lipid handling. In fasted animals, there were no differences in intestinal TG levels between wild-type and *Gpat3*$^{-/-}$ mice. However, TG content was significantly elevated in the ileum of the *Gpat3*$^{-/-}$ mice in the fed state (314 ± 27 and 606 ± 102 mg/g in wild-type and G*pat3*$^{-/-}$ mice, respectively, $p < 0.05$) (Fig. 3*A*). No differences in intestinal phospholipid or cholesterol content were found in either setting (data not shown). An oral olive oil challenge was performed, and as expected, plasma TG levels rapidly increased and returned to baseline in both wild-type and G*pat3*$^{-/-}$ mice. Baseline fasting TG levels were identical in both groups. However, at 90 and 120 min post-dose plasma TG levels were significantly reduced in G*pat3*$^{-/-}$ mice (Fig. 3*B*). Titration of the olive oil bolus revealed that a dose of 15 ml/kg was required to elicit this phenotype. This dose of lipid is in line with previous reports (20, 21) but higher than that used in studies examining the role of MGAT2 and DGAT1 in fat absorption (~4–8

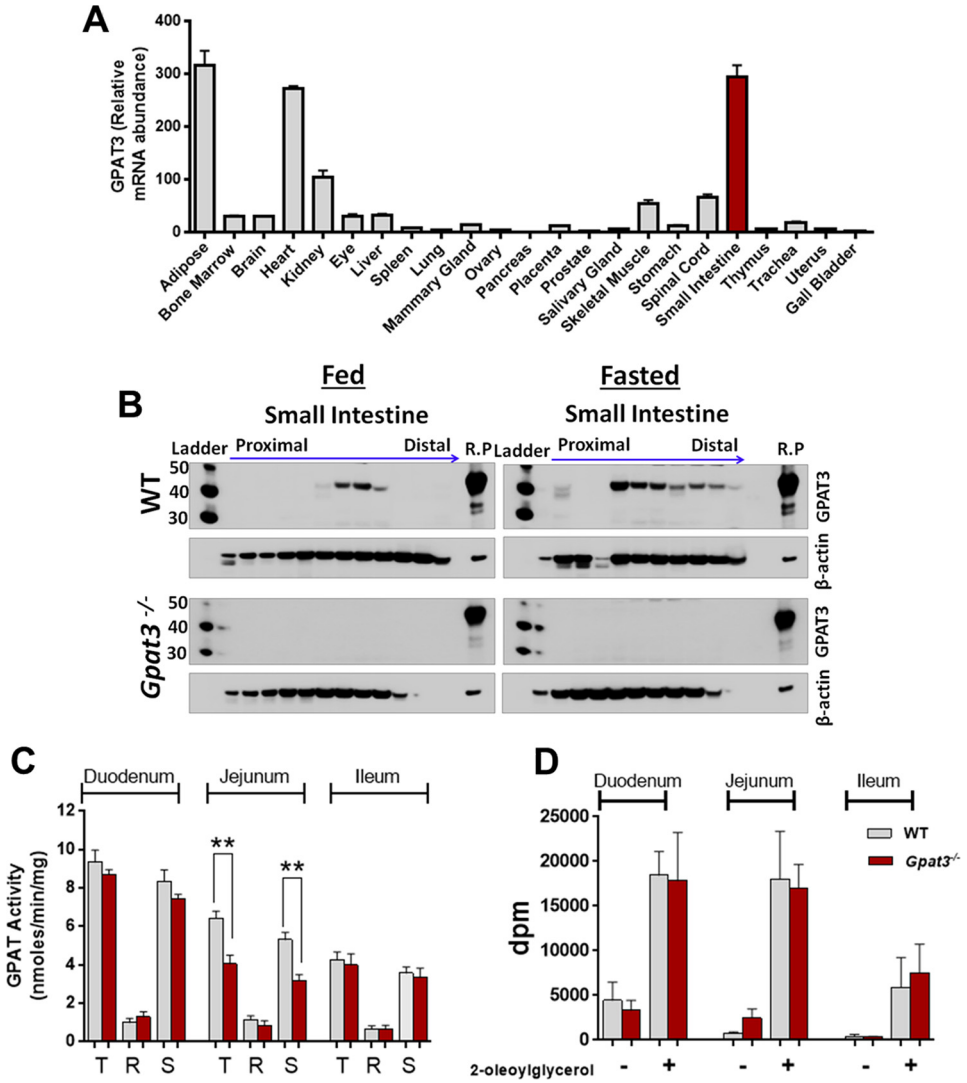

FIGURE 1. **GPAT3 is abundantly expressed and active in the small intestine.** *A*, gene expression analysis showing GPAT3 mRNA distribution in mouse tissues. Relative abundance in different tissues is normalized to the liver. Data are the mean ± S.E. from technical replicates. *B*, wild-type and *Gpat3*$^{-/-}$ mice were maintained on regular chow diet and either fed continuously or fasted (6 h) before sacrifice. The entire small intestine from the pylorus to the ileocecal junction was harvested and divided into 2.5-cm segments. GPAT3 protein expression was determined by Western immunoblotting in microsomal fractions from each segment with GPAT3 recombinant protein (*R.P*) as control. *C*, the entire small intestine was removed from fasted wild-type (*WT*) and *Gpat3*$^{-/-}$mice, divided into three equal segments which were designated (proximal to distal) duodenum (*D*), jejunum (*J*), and ileum (*I*), and mucosa was collected by scraping the mucosa from the underlying the muscularis mucosae. Microsomes were isolated, and total (*T*), NEM-resistant (*R*), and NEM-sensitive (*S*) GPAT activity was determined. Data are the mean ± S.E. ($n = 5$). **, $p < 0.005$ by one-way analysis of variance followed by Newman-Keuls multiple comparison test. *D*, MGAT activity was determined in the same mucosal sections as above in the presence (+) or absence of (−) 2-oleoylglycerol as reaction controls.

ml/kg) (8, 32). As such, these findings may be most relevant to conditions where large amounts of fat are ingested.

To further characterize this phenotype, plasma lipoprotein clearance was blocked by administering poloxamer 407, and tracer studies were performed *in vivo* using [^{3}H]triolein combined with an oral olive oil bolus. As expected, wild-type mice displayed accumulation of radiolabeled lipid in the plasma; however, the rate of appearance was significantly reduced in *Gpat3*$^{-/-}$ mice (Fig. 3*C*). Plasma FPLC fractionation showed reduced radiolabel associated with TG-rich lipoproteins (*fractions 5–10*, Fig. 3*D*). There was no difference in fecal tracer counts between the groups (data not shown). Distribution of radiolabeled lipid throughout the small intestine showed increased ^{3}H-labeled lipids in the jejunal portion of the small intestine accompanied by decreased lipid in the proximal segments (Fig. 3*E*).

To further examine the effects on the intestinal function, immunohistochemistry and electron microscopy were performed on the jejunum. Histology revealed extensive lipid droplet accumulation within the enterocytes of both wild-type and G*pat3*$^{-/-}$ mice. Although wild-type mice showed marked lipid staining in the lamina propria, *Gpat3*$^{-/-}$ mice exhibited a striking reduction in transitory lipids (Fig. 4*A*). Histological scoring confirmed that the *Gpat3*$^{-/-}$ mice, compared with the wild-type animals, exhibited significantly lower lipids in the lamina propria and intercellular space *versus* total amount of lipids present in the jejunal segments (Fig. 4*B*). Electron microscopy using TEM for single cell analysis revealed reduced trafficking of lipids, presumably chylomicrons in the basolateral surface of the enterocytes in the *Gpat3*$^{-/-}$ mice compared with the wild-type mice (Fig. 4*C*). Collectively, these observations suggest that GPAT3 deficiency results in the temporal accumu-

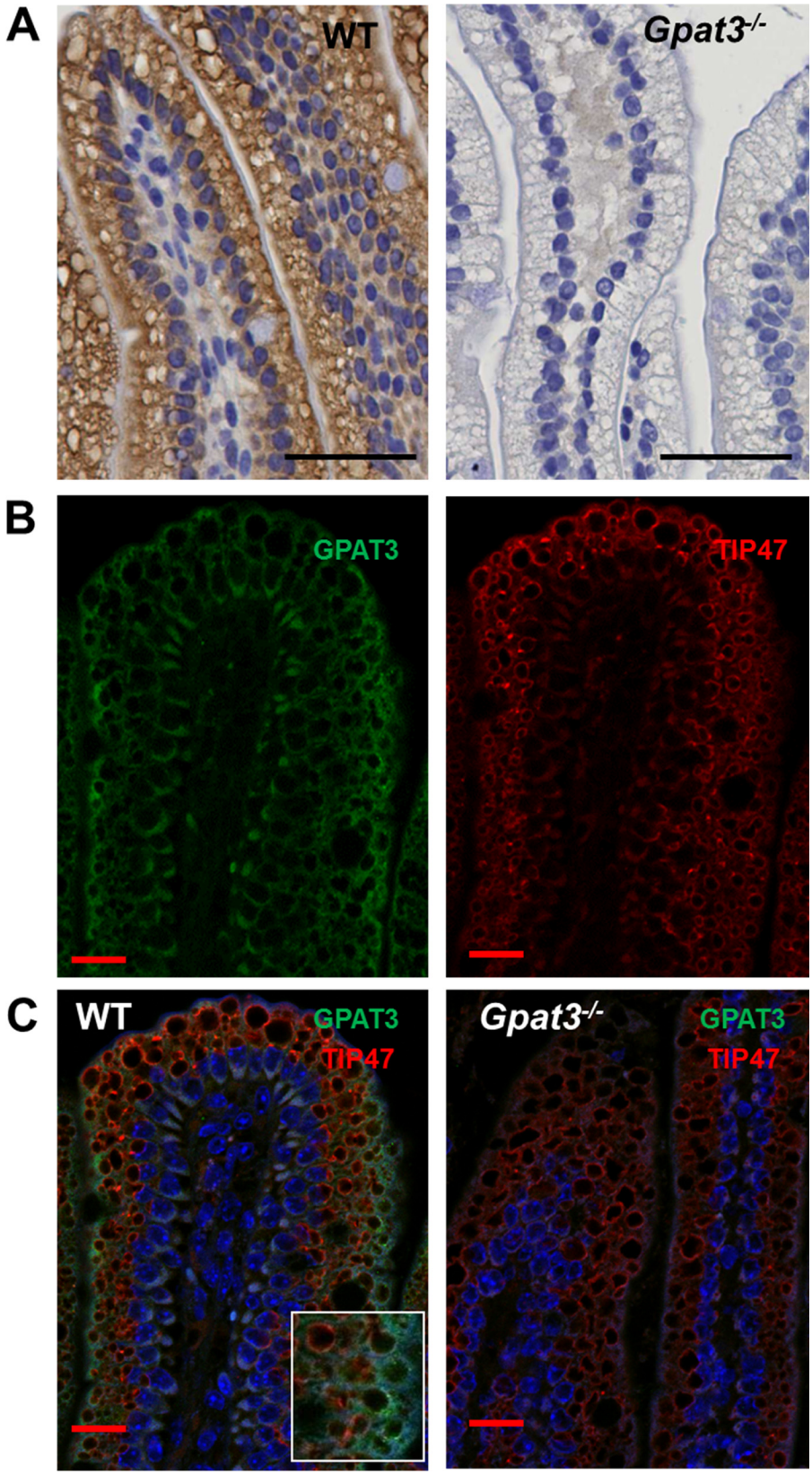

FIGURE 2. **GPAT3 is expressed in the absorptive epithelial cells of the small intestine.** Animals were maintained on standard chow and fasted for 6 h before administration of an oral olive oil bolus. Small intestines were collected 2 h post-dose as described in Fig. 1. *A*, immunohistochemistry of a representative jejunal segment showing GPAT3 protein expression and localization in WT (*left panel*) and *GPAT3*-null (*right panel*) enterocytes. *Scale bars* = 50 μm. *B*, individual immunofluorescence staining for GPAT3 (*green*, *left panel*) and TIP47 (*red*, *right panel*) in wild-type intestinal epithelium. *C*, merged staining for GPAT3 (*green*) and TIP47 (*red*) in wild-type (*left panel*) and *Gpat3*$^{-/-}$ (*right panel*) intestinal epithelium. Nuclei are stained *blue* with DAPI (4′,6-diamidino-2-phenylindole). *Scale bars* = 20 μm.

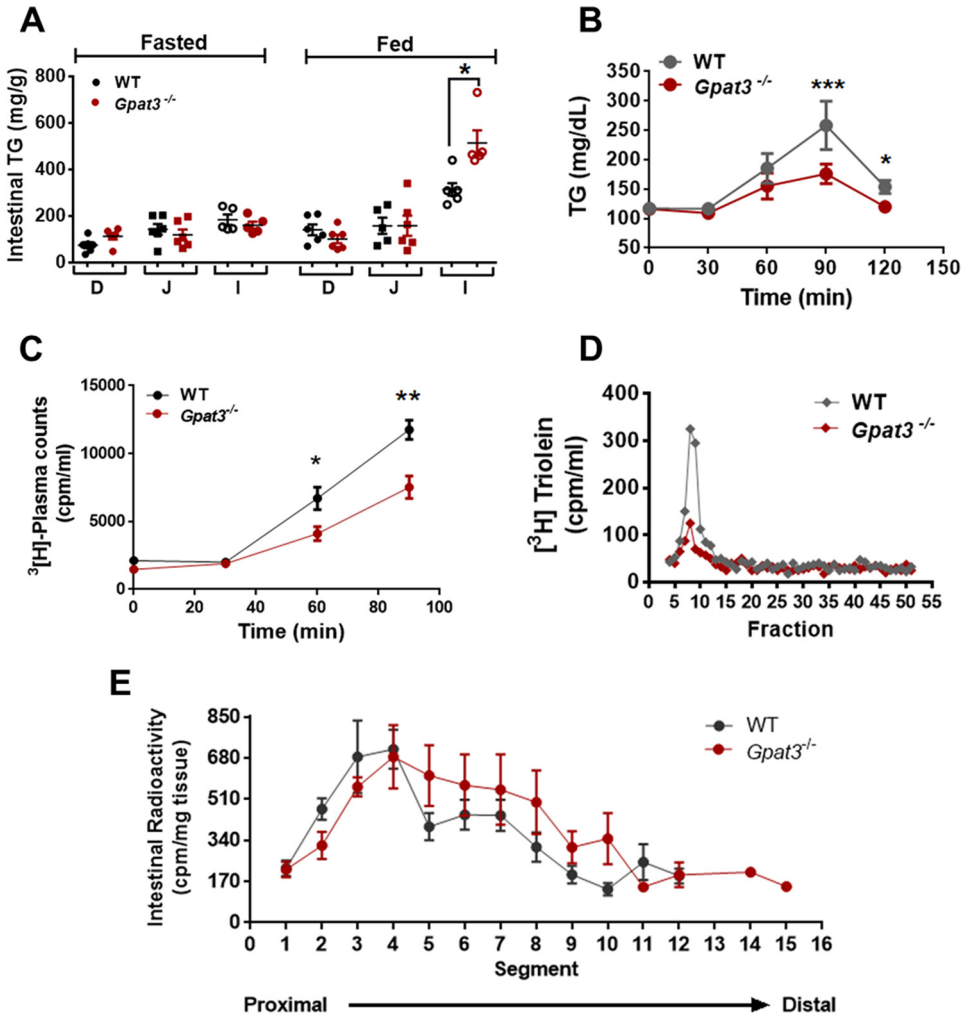

FIGURE 3. **Intestinal lipid absorption is dysregulated in *Gpat3*$^{-/-}$ mice.** *A*, TG content in the small intestine from wild-type and *Gpat3*$^{-/-}$ mice allowed chow *ad libitum* (*Fed*) or fasted (6 h, *Fasted*) before sacrifice. TG levels in duodenum (*D*), jejunum (*J*), and ileum (*I*) are shown. *B*, plasma TG excursion after an oral lipid bolus. Mice were fasted (6 h) before receiving olive oil (15 ml/kg, *per os*). Plasma TG was determined on blood drawn from the lateral tail vein at the indicated times after olive oil gavage. Data are the mean ± S.E. ($n = 8$). *, $p < 0.05$; ***, $p < 0.001$ by Student's *t* test. *C–E*, mice were fasted (6 h) and administered poloxamer 407 (10 mg/kg, *intraperitoneal*), and 30 min later animals received olive oil containing [^{3}H]triolein. *C*, plasma tracer counts from tail bleeds at the indicated times after olive oil gavage. *D*, tracer incorporation in different lipoprotein population determined by measuring counts after gel filtration. *E*, distribution of tracer uptake along the small intestine axis from pylorus (proximal) to the ileocecal junction (distal) in 2.5-cm sections 2 h post-dose.

lation of lipids within the enterocytes during increased dietary lipid loaded states.

GPAT3 Deficiency Results in Alterations in Lipid Metabolism and Enteroendocrine Hormone Production—In the *Gpat3*$^{-/-}$ mice, the blunted postprandial plasma TG excursion after olive oil bolus was associated with increases in duodenal, jejunal, and ileal lipid content (Fig. 5*A*). Similar to mice maintained on standard chow, *Gpat3*$^{-/-}$ mice administered an olive oil bolus exhibited elevated TG levels in the distal region of the small intestine (Figs. 3*A* and 5*A*). In line with GPAT3 protein expression, the *Gpat3* gene was most abundantly expressed in jejunum (Fig. 5*B*). The loss of *Gpat3* expression was accompanied by a compensatory increase in *Gpat4* mRNA (Fig. 5*C*). Small intestinal levels of FFAs were modestly but significantly elevated in *Gpat3*$^{-/-}$ compared with the wild-type animals (Table 1). Interestingly, although the relative abundance of long chain polyunsaturated fatty acids such as eicosapentaenoic (C20:5), docosapentaenoic (C22:5), and docosahexaenoic acid (C22:6) was low throughout the small-intestine, *Gpat3*$^{-/-}$ mice had reduced levels of these lipids compared with the wild type in the jejunum and ileum (Table 1). The changes in TG and FFA were accompanied by significant increases in intestinal long chain acylcarnitines in *Gpat3*$^{-/-}$ mice (Table 2). There were no changes in short chain acylcarnitines (data not shown). These data accompanied with the increases in total FFA levels suggest increased intestinal fatty acid oxidation in the *Gpat3*$^{-/-}$ mice.

To explore any potential adaptive changes that take place in the intestinal mucosa of *Gpat3*$^{-/-}$ mice, we evaluated the expression of multiple genes encoding proteins involved in lipid metabolism. Compared with the wild-type mice, significant decreases in the expression of *Dgat1*, *Dgat2*, and *Mgat2* were evident in *Gpat3*$^{-/-}$ jejunum (Fig. 5*D*). In line with increased FFA and long-chain acyl carnitine levels, genes encoding proteins involved in fatty acid oxidation, such as carnitine palmitoyltransferase 1 (*Cpt1a*, ~1.3-fold), acyl-CoA thioesterase (*Acot1*, ~4-fold), and acyl-CoA oxidase 1 (*Acox1*, ~3.5-fold) were significantly induced in *Gpat3*$^{-/-}$ mice (Fig. 5*D*). The level of mRNA encoding fibroblast growth factor 15 (*Fgf15*) and

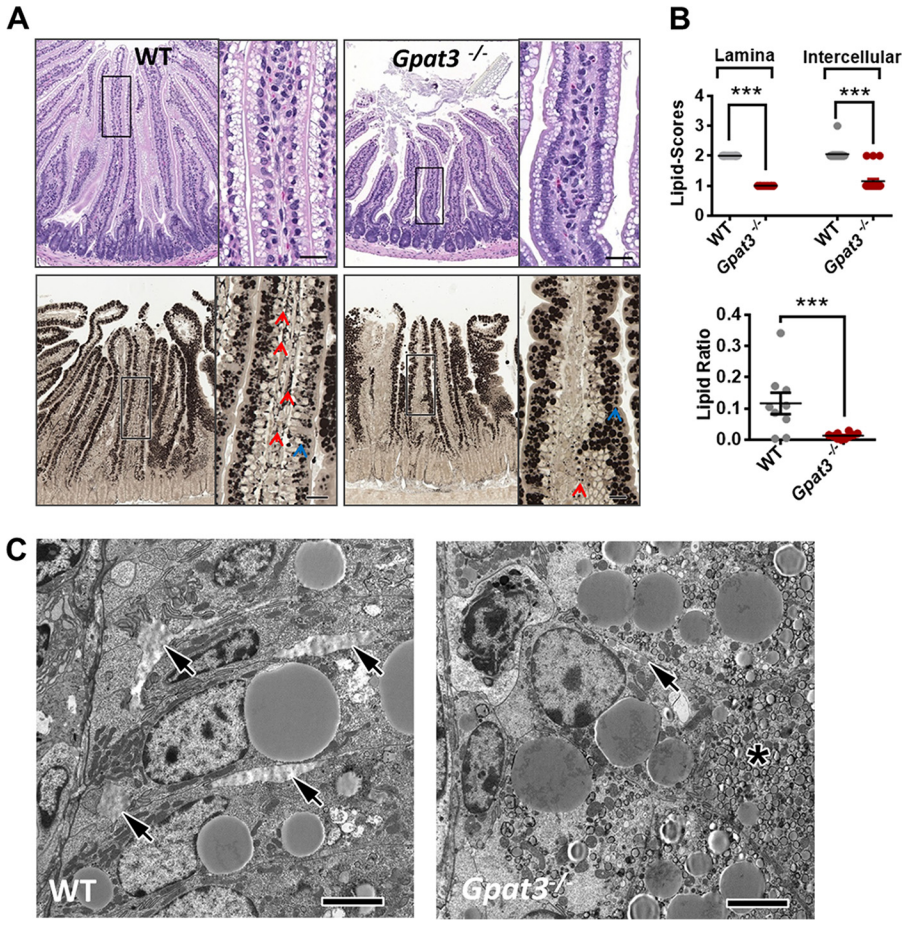

FIGURE 4. **Lipid uptake and distribution in the intercellular space of the intestinal villi.** Mice were fasted (6 h) before dosing with a single oral bolus of olive oil. Small intestinal segments were collected 2 h post-dose. *A*, H&E staining (*top panel*, 10×) and osmium paraphenylenediamine staining (*bottom panel*, 10×) of the jejunal segments after olive oil feeding in wild-type and *Gpat3*$^{-/-}$ mice. *Insets* (40X, scale = 25 μm) show magnified images of lipid traffic in the lamina propria (*red arrows*) in the wild-type but not in the *Gpat3*$^{-/-}$ mice with respect to lipids retained within the enterocytes (*blue arrow*). *B*, lipid scores in the lamina propria and intercellular space (*top panel*); ratio of lipids in the intercellular space with respect to the total lipids in the intestinal epithelium (*bottom panel*). Scores were assigned based on whole slide analysis for $n = 10$ animal/group. *C*, representative TEM electron micrographs of epithelium in the jejunal intestinal villi. Extracellular chylomicrons (*arrows*) are prominent in WT (*A*, *left panel*) compared with *Gpat3*$^{-/-}$ (*B*, *right panel*). Accumulation of microvesicular bodies (*asterisk* (*)) were present in *Gpat3*$^{-/-}$. *Scale bars* = 4 μm.

small heterodimer partner (*Shp*), which are both central components in bile acid homeostasis, were elevated by ~2.5–3-fold. Expression of the nuclear receptor peroxisome proliferator-activated receptor α (*Pparα*) was significantly decreased in *Gpat3*$^{-/-}$ mice compared with the wild-type animals (Fig. 5*D*).

Because we observed deregulated lipid secretion and accumulation of TG in the enterocytes of *Gpat3*$^{-/-}$ mice after an oral lipid bolus, we examined the effect of GPAT3 deletion on the expression of apolipoprotein A4 (*Apoa4*) and glucose-dependent insulinotropic polypeptide (*Gip*). The *Gip* and *Apoa4* genes are preferentially expressed in the small intestine where the synthesis and secretion of these proteins is reported to be modulated by dietary lipids (33–35). Expression of the *Apoa4* and *Gip* genes was significantly induced throughout the small intestine in *Gpat3*$^{-/-}$ mice compared with the wild-type animals (Fig. 5*E*). Interestingly, expression of the glucagon gene (*Gcg*), which encodes glucagon-like peptide-1 (GLP-1) in the gut, was also increased in the intestine of *Gpat3*$^{-/-}$ mice (Fig. 5*E*). *Gpat3*$^{-/-}$ plasma GIP levels revealed a ~2-fold increase compared with the wild-type animals when either fasted for 6 h (100 ± 17 and 201 ± 38 pg/ml in wild-type and *Gpat3*$^{-/-}$mice, respectively, $p < 0.05$) or allowed food *ad libitum* (105 ± 14 and 216 ± 27 pg/ml in wild-type and *Gpat3*$^{-/-}$mice, respectively, $p < 0.01$) (Fig. 5*F*). When mice were gavaged with olive oil there was a marked increase in circulating GIP levels; however, the genotype effect apparent in mice maintained on standard chow was lost (Fig. 5*G*). We were unable to detect any changes in total GLP in either setting (data not shown).

Attenuation of Postprandial Triglyceride Excursion Is Secondary to Decreased Secretion and Not Differential Absorption from Intestinal Lumen—To better understand the effects of GPAT3 deletion on lipid absorption and secretion, we performed a series of pulse-chase studies using [^{3}H]oleate and [^{14}C]cholesterol in *ex vivo* cultures of murine enterocytes derived from wild-type and *Gpat3*$^{-/-}$ mice (Fig. 6*A*). Radiolabeled oleate uptake into primary enterocytes, as determined by [^{3}H]oleate incorporation into the cellular lipid fraction, was not significantly affected by loss of GPAT3 (Fig. 6*B*, *inset*). However, when the distribution of [^{3}H]oleate into cellular lipids was examined, a marked redistribution was apparent. Thus, in *Gpat3*$^{-/-}$ enterocytes, incorporation of [^{3}H]oleate into TG was reduced with a parallel increase in the production of ^{3}H-labeled

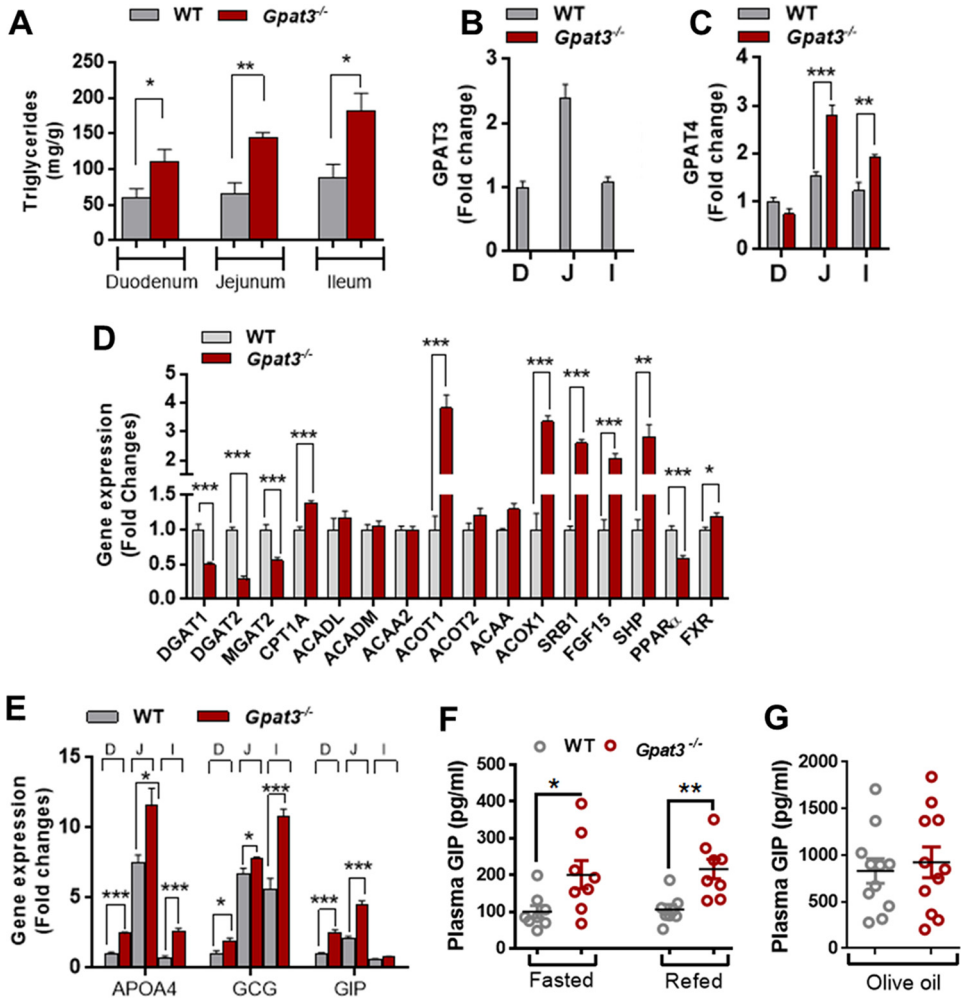

FIGURE 5. **Effects of GPAT3 deletion on intestinal lipid profile, gene expression, and gut nutrient sensing.** Fasted mice were gavaged with olive oil and sacrificed 2 h later. The small intestine was harvested, and mucosa was collected from the indicated segments for quantification of triglyceride levels or gene expression. *A*, TG levels in the duodenum (*D*), jejunum (*J*), and ileum (*I*). GPAT3 mRNA (*B*) and GPAT4 mRNA (*C*) expression levels along the small intestine are shown. Data are expressed as -fold change relative to jejunum. Shown is jejunal (*D*) and entire small intestine (*E*) expression of genes involved in gut lipid metabolism and nutrient sensing. Data are expressed as -fold change relative to values determined in wild-type jejunum. *DGAT1*, diacylglycerol *O*-acyltransferase 1; *DGAT2*, diacylglycerol *O*-acyltransferase 2; *MGAT2*, monoacylglycerol *O*-acyltransferase 2; *CPT1A*, carnitine palmitoyltransferase 1a, liver; *ACADL*, acyl-coenzyme A dehydrogenase, long chain; *ACADM*, acyl-coenzyme A dehydrogenase, medium chain; *ACAA2*, acetyl-coenzyme A acyltransferase 2; *ACOT1*, acyl-CoA thioesterase 1; *ACOT2*, acyl-CoA thioesterase 2; *ACAA*, acetyl-coenzyme A acyltransferase 1B; *ACOX1*, acyl-coenzyme A oxidase 1, palmitoyl; *SRB1*, scavenger receptor class B, member 1; *FGF15*, fibroblast growth factor 15; *SHP*, nuclear receptor subfamily 0, group B, member 2; *PPARα*, peroxisome proliferator-activated receptor α; *FXR*, NR1H4, nuclear receptor subfamily 1, group H, member 4; *APOA4*, apolipoprotein A-IV; *GCG*, glucagon. *F*, plasma total GIP in mice that were either fasted for 6 h (*Fasted*) or fasted and then refed (*Refed*) with standard laboratory chow. *G*, plasma GIP in fasted mice after an olive oil gavage. Data are the mean ± S.E. *, $p < 0.05$; **, $p < 0.01$; ***, $p < 0.001$ by Student's *t* test.

TABLE 1

Intestinal FFA profile determined by LC-MS analysis

Animals were administered an oral olive oil bolus (15 ml/kg) after a 6-h fast. Before the study wild type and animals were maintained on standard laboratory chow. Data are the mean ± S.D.

	Duodenum		Jejunum		Ileum	
Species	Wild type ($n = 6$)	*Gpat3*$^{-/-}$ ($n = 7$)	Wild type ($n = 7$)	*Gpat3*$^{-/-}$ ($n = 6$)	Wild type ($n = 7$)	*Gpat3*$^{-/-}$ ($n = 6$)
14:0	230 ± 41	359 ± 98	413 ± 90	584 ± 140[a]	623 ± 105	949 ± 82[a]
16:0	12,462 ± 2,286	14,151 ± 1,906	12,517 ± 1,362	14,505 ± 2,812	12,428 ± 2,513	14,961 ± 2,259
16:1	1,319 ± 183	1,689 ± 321[a]	1,345 ± 147	1,916 ± 590[a]	1,685 ± 58.0	2,542 ± 393[b]
18:0	6,083 ± 434	6,038 ± 540	6,433 ± 400	6103 ± 331	5,829 ± 624	5,033 ± 654
18:1	36,157 ± 9,571	37,852 ± 8,491	24,428 ± 5431	27,015 ± 6128	17,849 ± 1,649	15,762 ± 1665
18:2	8,142 ± 964	8,587 ± 1144	6,529 ± 632	7,226 ± 1446	6244.5 ± 579	7,451 ± 1028
20:4	1,520 ± 572	1,266 ± 623	1,113 ± 206	907 ± 168	1,114 ± 325	701 ± 120
20:5	179 ± 58	122 ± 91	132 ± 11	90 ± 19[b]	132 ± 30	92 ± 17[a]
22:5	115 ± 38	95 ± 48	126 ± 23	110 ± 334	146 ± 34	108 ± 26
22:6	763 ± 252	517 ± 318	640 ± 179	432 ± 134[a]	640 ± 165	368 ± 136[c]

[a] $p < 0.05$, as determined by Student's *t* test.
[b] $p < 0.001$, as determined by Student's *t* test.
[c] $p < 0.01$, as determined by Student's *t* test.

TABLE 2

Intestinal long chain acylcarnitine profile

Animals were administered an oral olive oil bolus (15 ml/kg) after a 6-h fast. Before the study wild-type and animals were maintained on standard laboratory chow. Data are the mean ± S.D.

	Duodenum		Jejunum		Ileum	
Species	Wild type ($n = 6$)	*Gpat3*$^{-/-}$ ($n = 7$)	Wild type ($n = 7$)	*Gpat3*$^{-/-}$ ($n = 6$)	Wild type ($n = 7$)	*Gpat3*$^{-/-}$ ($n = 6$)
14:0	75.6 ± 21	73.6 ± 15	45.2 ± 12	73.5 ± 33[a]	54.5 ± 18	83.4 ± 23[a]
16:0	124 ± 25	111 ± 28	92.9 ± 18	112 ± 30[a]	1219 ± 19	126 ± 13
16:1	6.2 ± 1.1	5.2 ± 1.0	4.4 ± 0.61	4.8 ± 0.98	5.4 ± 0.81	5.1 ± 0.46
18:2	31.1 ± 7.2	23.0 ± 7.9[a]	18.5 ± 5.6	22.4 ± 8.0[a]	30.5 ± 7.8	25.6 ± 5.7
18:1	105 ± 19	92.8 ± 30	85.3 ± 26	118 ± 45[a]	98.2 ± 19	105 ± 21
18:0	106 ± 25	119 ± 20	98.6 ± 34	150 ± 65[a]	94.0 ± 31	161 ± 28[b]
20:6	3.9 ± 0.71	3.3 ± 0.42	4.4 ± 0.28	4.0 ± 1.01	4.3 ± 0.61	3.5 ± 0.45
20:5	2.4 ± 0.58	1.8 ± 0.36[a]	1.99 ± 0.25	1.9 ± 0.45	2.2 ± 0.71	1.6 ± 0.30
20:4	6.1 ± 0.54	5.4 ± 1.3	5.3 ± 0.57	5.9 ± 0.75	7.5 ± 1.1	6.5 ± 1.1
20:3	1.4 ± 0.25	1.3 ± 0.31	1.4 ± 0.18	1.3 ± 0.27	2.1 ± 0.41	1.7 ± 0.30
20:2	5.6 ± 0.85	5.6 ± 1.2	6.3 ± 1.7	6.9 ± 2.0	5.9 ± 1.6	6.5 ± 1.1
20:1	81.0 ± 8.2	84.3 ± 22	81.8 ± 24	85.3 ± 28	67.5 ± 16	74.1 ± 8.0
20:0	17.6 ± 4.5	16.9 ± 4.7	14.4 ± 4.1	15.2 ± 4.3	12.3 ± 3.8	10.5 ± 1.6
22:0	6.2 ± 1.9	5.9 ± 1.9	5.00 ± 0.90	4.7 ± 1.3	4.9 ± 1.5	3.5 ± 0.45

[a] $p < 0.05$, as determined by Student's *t* test.
[b] $p < 0.01$, as determined by Student's *t* test.

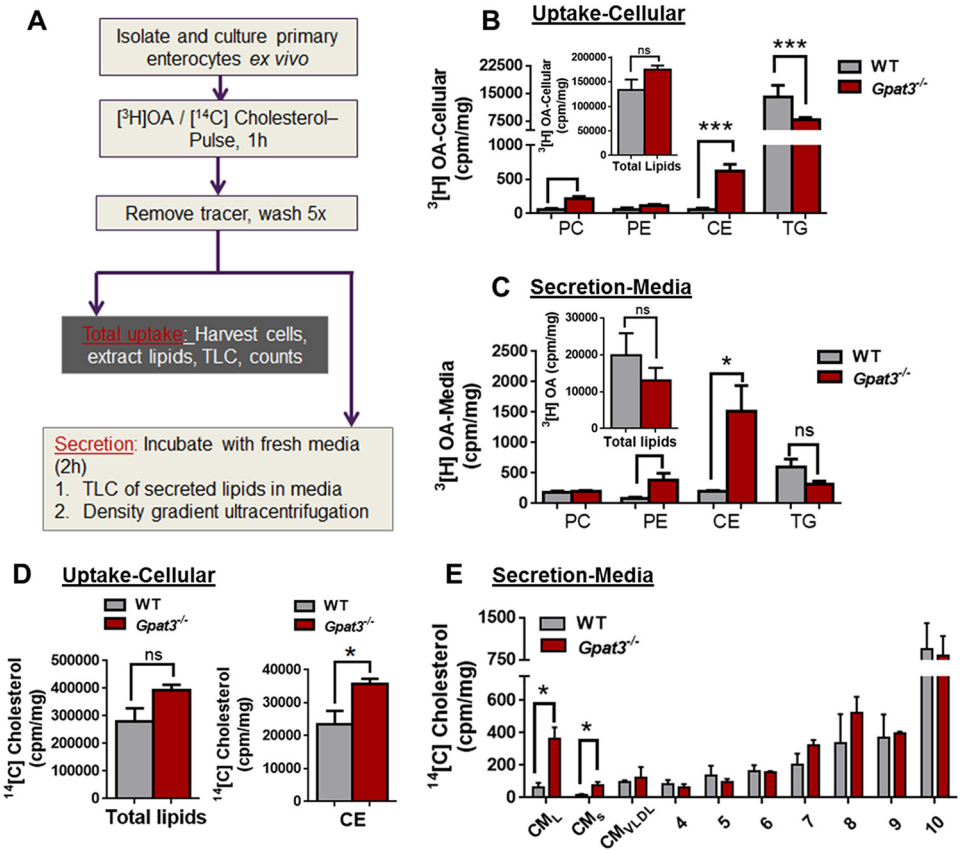

FIGURE 6. ***Ex vivo* flux analysis in primary enterocytes from wild-type and *Gpat3*$^{-/-}$ mice.** *A*, flowchart of *ex vivo* uptake or secretion studies using dual radioisotope. *B*, distribution of [^{3}H]oleic acid (*OA*) in the intracellular lipid pool. *PC*, phosphatidylcholine. *PE*, phosphatidylethanolamine. The *inset* shows total cellular lipid counts. *C*, total lipids secreted in the media (*inset*) and distribution of [^{3}H]oleic acid in the secreted pool. *D*, [^{14}C]cholesterol incorporation in total cellular lipids (*left panel*) and incorporation of tracer in intracellular CE. Total cellular lipids were determined by liquid scintillation counting, whereas the incorporation into TG and phospholipid was monitored by TLC. *ns*, not significant. *E*, [^{14}C]cholesterol counts in media fractions subject to density gradient ultracentrifugation. Large chylomicrons, CM_L (floatation coefficient, Sf > 400); small chylomicrons, CM_S (Sf = 60–400); CM_{VLDL} (Sf = 20–60); fraction 4–10 representing HDL. Data are the mean ± S.E. ($n = 4$). *, $p < 0.05$; ***, $p < 0.001$ by either one-way analysis of variance followed by Newman-Keuls multiple comparison test or Student's *t* test.

cholesteryl ester (Fig. 6*B*). Secretion of ^{3}H-labeled lipid was examined during the chase period. There were no significant differences in total lipid secretion (Fig. 6*C*, *inset*). In enterocytes derived from the wild-type mice, TG was the primary lipid species secreted into the media; however, in *Gpat3*$^{-/-}$ enterocytes TG secretion was reduced, and there was a compensatory increase in the secretion of labeled cholesteryl ester (CE) and phosphatidylethanolamine (*PE*) (Fig. 6*C*). When [^{14}C]cholesterol was used as the tracer, a significant increase in the production of intracellular [^{14}C]CE in *Gpat3*$^{-/-}$cells was observed

(Fig. 6*D*). Finally, media were collected, and lipoprotein fractions were separated by density gradient fractionation. [^{14}C]Cholesterol secretion in the large (floatation coefficient, Sf > 400) and small (Sf = 60–400)) chylomicron (CM_L, CM_S) population was significantly increased in media derived from *Gpat3*$^{-/-}$ enterocytes. CE secretion onto HDL (fractions 4–10) was unaffected by disruption of GPAT3 (Fig. 6*E*). Taken together these data suggest that the reduced appearance of TG in the plasma after an oral lipid bolus in *Gpat3*$^{-/-}$ mice was as a result of reduced TG secretion, whereas the uptake of FFA from the intestinal lumen remains largely intact. In the absence of GPAT3, excess FFA derived either directly from luminal lipid absorption or liberated within the cell after hydrolysis of stored lipid is esterified with cholesterol, thereby protecting the cell from the accumulation of potentially harmful FFA. Ultimately, the excess CE produced in GPAT3-null mice is secreted on CM particles resulting in the production of cholesterol-rich CM.

GPAT3 Abrogation Attenuated Plasma Cholesterol, Exacerbated Hepatic Steatosis, and Altered Cholesterol-Bile Acid Homeostasis—Based on the findings that loss of GPAT3 in the intestine results in altered lipid secretion and the dysregulation of multiple genes involved in enteric fatty acid and bile acid homeostasis, we further evaluated the physiological role of GPAT3 in whole-body lipid metabolism in mice fed a high fat, high cholesterol WTD for 4 weeks. This diet contained 0.2% cholesterol (w/w) and 42% kcal from fat. WTD feeding stimulated significant but comparable body weight gain in both wild-type and *Gpat3*$^{-/-}$ mice (Fig. 7*A*). No changes in fasted plasma TG were observed (Fig. 7*B*); however, *Gpat3*$^{-/-}$ mice showed decreased total plasma cholesterol under both chow and WTD-fed conditions (Fig. 7*B*). Size fractionation of plasma lipoproteins by gel filtration to analyze lipid distribution in different lipoprotein classes showed no differences in VLDL-TG (data not shown); however, lower HDL-cholesterol was observed in the *Gpat3*$^{-/-}$ mice (Fig. 7*D*). Plasma alanine transaminase (*ALT*) levels, a marker of liver damage, were increased in *Gpat3*$^{-/-}$ mice compared with wild-type mice (Fig. 7*E*). Both wild-type and *Gpat3*$^{-/-}$ mice fed on WTD exhibited pronounced hepatic steatosis compared with the chow-fed wild-type and *Gpat3*$^{-/-}$ mice; however, the livers of WTD-fed *Gpat3*-null mice accumulated significantly more lipid compared with the WTD-fed wild-type livers. HPLC analysis showed increases in TG, DAG, and CE in WTD-fed *Gpat3*$^{-/-}$ cohorts compared with the wild-type animals (Fig. 7, *F* and *G*). The livers of *Gpat3*$^{-/-}$ mice exhibited significantly high levels of cholesteryl ester when maintained on a WTD (Fig. 7*H*).

In the liver biliary cholesterol secretion or catabolism to bile acids represent the primary routes for elimination for excess hepatic cholesterol. Given the elevated hepatic CE (Fig. 7*H*) and dysregulation of the *Fgf15* and *Shp* genes in the small intestine of *Gpat3*$^{-/-}$ mice (Fig. 5*D*), we examined the effects of GPAT3 deletion on bile acid homeostasis. Wild-type and *Gpat3*$^{-/-}$ mice exhibited similar levels of plasma total bile acids (TBAs) when maintained on standard chow (Fig. 7*I*). WTD feeding resulted in a ~2.6-fold reduction in plasma TBAs in wild-type mice; however, plasma TBAs in *Gpat3*$^{-/-}$ cohorts were maintained at a comparable level with that observed in chow-fed animals (Fig. 7*I*). In contrast, hepatic TBA was elevated after WTD feeding, and the level was significantly (~1.9-fold) lower in *Gpat3*$^{-/-}$ mice (Fig. 7*J*). These data suggest that disruption of the *Gpat3* gene results in alterations of entero-hepatic bile acid homeostasis.

Discussion

For more than 40 years it has been recognized that the monoacylglycerol pathway is the primary route for the resynthesis of dietary triacylglycerol in the enterocyte. However, MGAT2-deficient mice exhibit minimal quantitative effects on lipid absorption (8). These data combined with earlier studies suggest the existence of alternative, MGAT-independent pathways for lipid absorption (3–7). In this study we utilized *Gpat3*$^{-/-}$ mice to characterize an intestinal glycerol 3-phosphate pathway.

In mammals, four distinct GPAT genes have been identified (12). GPAT3 was initially characterized by Cao *et al.* (17) and shown to be induced in adipocytes after exposure to the PPARα agonist rosiglitazone. The *Gpat3* gene was found to be highly expressed in adipose and small intestine. Our study demonstrates that the GPAT3 protein is abundantly expressed in the enterocytes of the jejunum where it is strongly up-regulated during fasting. Targeted disruption of the *Gpat3* gene resulted in ~40% reduction in total and NEM-sensitive microsomal GPAT activity in the jejunum. In line with the protein expression data, microsomal GPAT activity was preserved in the duodenum and ileum of *Gpat3*$^{-/-}$ mice. These data suggest that either GPAT4 is the primary contributor to GPAT activity in the duodenum and ileum or that there is a compensatory increase in *Gpat4* activity or another unidentified GPAT after loss of GPAT3 activity. Although the majority of GPAT3 staining within the enterocyte appeared to be diffuse, dense punctate staining of GPAT3 was evident in proximity to the surface of the lipid droplet after an oral lipid bolus. Although we did not perform a detailed analysis of the subcellular localization of GPAT3, it is possible that, in analogy to closely related GPAT4, the GPAT3 protein relocalizes from the endoplasmic reticulum to the surface of the lipid droplet upon cellular lipid loading (36).

The intestinal expression profile of GPAT3 suggests a role in intestinal lipid absorption. In support of this, *Gpat3*$^{-/-}$ mice exhibit a reduction in plasma TG excursion when administered an oral lipid bolus that was accompanied by increased accumulation of TG in enterocytes. There were no differences in intestinal TG levels between wild-type and *Gpat3*$^{-/-}$ mice when animals were fasted, and there was no evidence of fecal lipid loss after an acute lipid load. GPAT3-deficient mice displayed a modest increase in enteric free fatty acid levels that was paralleled by induction of multiple genes involved in fatty acid oxidation (*e.g. Cpt1a*, *Acot1*, *Acox1*) and elevations in acylcarnitines, suggesting an adaptive response to protect against the accumulation of non-esterified fatty acids. Although we observed increased TG accumulation in the small intestine of *Gpat3*$^{-/-}$ mice, there was a marked decrease in lipids in the lamina propria and intercellular space, suggesting that GPAT3 plays a role in chylomicron assembly or subsequent secretion into the lymph via the basolateral surface. This hypothesis was supported by a series of pulse-chase studies performed in

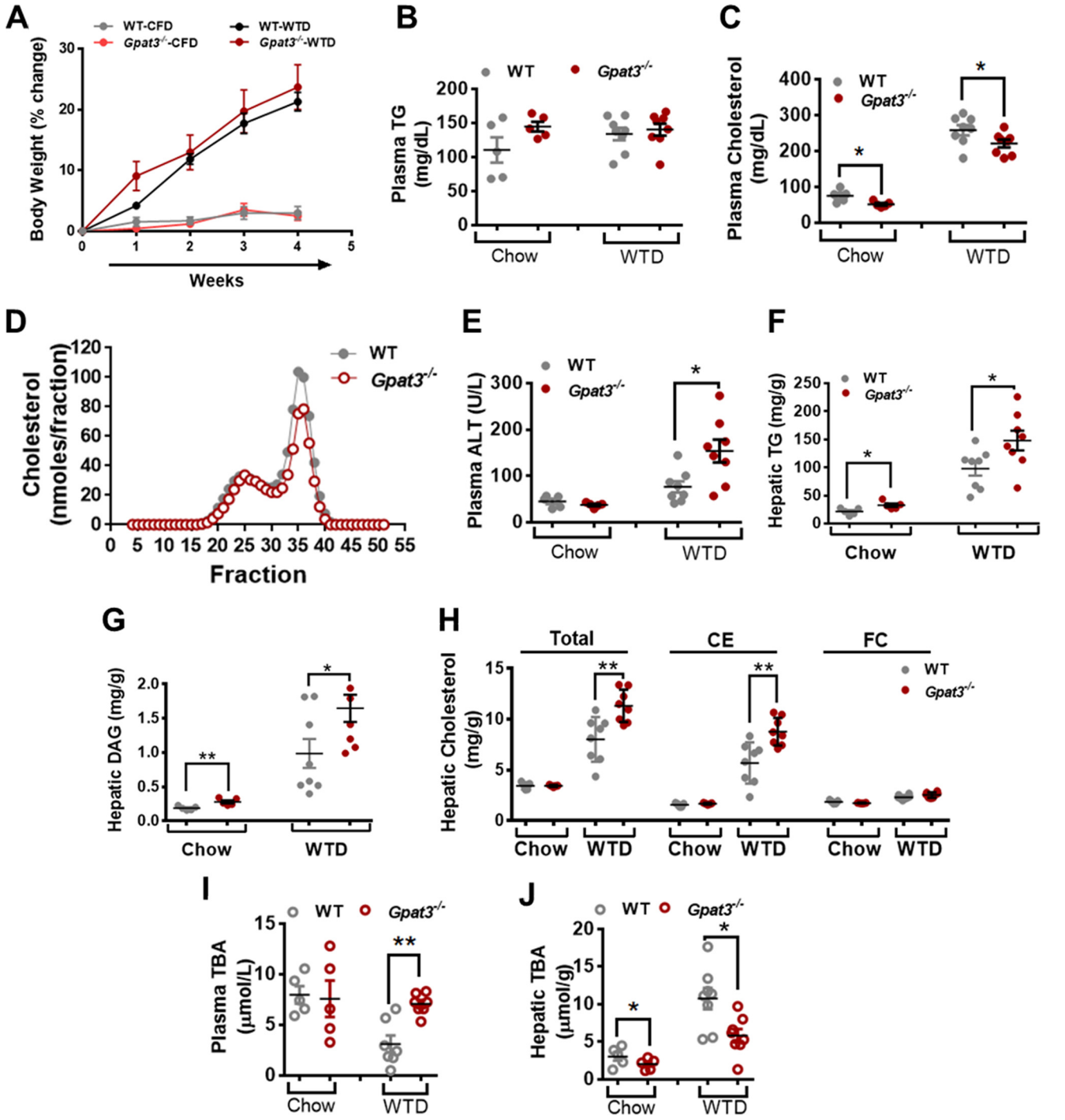

FIGURE 7. **Gpat3$^{-/-}$ mice exhibit dysregulated hepatic cholesterol and bile acid homeostasis.** WT and *Gpat3*$^{-/-}$ mice were fed a WTD for 4 weeks. Mice were fasted for 6 h on the day of sacrifice. *A*, body weight change (percent change calculated from initial weight) during the course of the diet. Plasma TG (*B*) and total plasma cholesterol (*C*) in chow- and WTD-fed animals. *D*, distribution of cholesterol in different plasma lipoprotein populations separated by FPLC. Plasma alanine transaminase (*ALT*) (*E*) and hepatic TG (*F*), DAG (*G*), and hepatic cholesterol (*CE*, cholesteryl ester; *FC*, free cholesterol) (*H*). Plasma (*I*) and hepatic total bile acids (*TBA*) (*J*) levels. All data are the mean ± S.E. ($n = 8$). *, $p < 0.05$; **, $p < 0.01$ by Student's *t* test.

enterocytes derived from wild-type and *Gpat3*$^{-/-}$ mice. Taken together, these data suggest that GPAT3 plays a role in multiple facets of intestinal lipid metabolism. Thus, in the face of elevated lipid levels, GPAT3 localizes to the CLD where it contributes to the short term storage of dietary lipids in the enterocyte. In addition, GPAT3 appears to be involved in the appropriate partitioning of lipid for the formation and secretion of chylomicrons, possibly through participation in a lipolysis reesterification process analogous to that proposed for VLDL secretion in the liver.

Overall, the intestinal phenotype observed in the *Gpat3*$^{-/-}$ is qualitatively similar to that observed in *Dgat1*$^{-/-}$ mice (8, 32, 37). Thus, *Dgat1*-null animals exhibited decreased plasma chylomicronemia after an oral lipid bolus and accumulate TG in the gut epithelia (32). Disruption of the *Dgat1* locus or pharmacological inhibition of DGAT1 is associated with an improved

metabolic profile upon high fat diet feeding, including decreased body weight gain, increased insulin sensitivity, and reduced hepatic lipid accumulation (32, 37–40). However, in contrast, when maintained on high fat diets, *Gpat3*$^{-/-}$ mice exhibit weight gain in line with wild-type animals and accumulate excess hepatic lipid in the form of TG, DAG, and CE. The reason for this difference is unclear; however, it could relate to divergent effects on enteroendocrine hormone release. Thus, although inhibition of DGAT1 is associated with suppression of GIP and robust increases in GLP-1 and the anorectic hormone peptide YY (PYY) (38, 41), loss of GPAT3 results in elevated levels of circulating GIP. We were unable to discern an effect on GLP-1 levels in *Gpat3*$^{-/-}$ mice. In preclinical models, increased exposure to dietary lipid is reported to increase GIP levels and mice containing a disrupted GIP receptor gene (*Gipr*$^{-/-}$) are protected from diet-induced obesity (42). The molecular mechanism underlying this observation could relate to difference in the expression of the *Gpat3* and *Dgat1* genes throughout the small intestine or the liberation of specific lipids after blockade of these enzymes (43).

In preliminary experiments we determined that an oral lipid bolus of 15 ml/kg olive oil was required to elicit significant differences between wild-type and *Gpat3*$^{-/-}$ mice in the plasma lipid excursion (data not shown). Although this degree of oral lipid-loading has been previously described (20, 21), it is markedly higher than the dose of olive oil (~4–8 ml/kg) required to delineate the role of MGAT2 and DGAT1 in fat absorption (8, 32). Thus, it appears that under normal physiological conditions, the GPAT3 pathway is a minor pathway for lipid absorption compared with the canonical MGAT2-DGAT1 pathway. It is possible that GPAT3 is a component of a rescue system that evolved to ensure efficient absorption of ingested lipid after a fat-rich meal. Alternatively, intestinal GPAT3 could play a role in the absorption of specific species. Notably, the acute lipid absorption studies we performed exclusively utilized olive oil, which is predominantly composed of oleate (C18:1) and, to a lesser extent, palmitate (C16:0).

In summary, we have characterized a role for GPAT3 in the regulation of intestinal lipid absorption. Targeted disruption of the *Gpat3* locus results in dysregulation of TG secretion from the small intestine.

Author Contributions—I. K. and B. G. provided the study concept and design, analysis, interpretation of data, drafting of the manuscript, and critical revision of the manuscript for important intellectual content. I. K., R. W. C., N. B V., K. K., T. C., W. F. B., and C. O. provided the acquisition of data, analysis, and interpretation of data. D. M. E. provided analysis and interpretation of data and critical revision of the manuscript for important intellectual content.

Acknowledgments—We acknowledge Matthew Gorgoglione, Julie Purkal, Collin Crowley, Trenton Ross, Darla Dash, Paul Amor, Sylvie Perez, Adhiraj Lanba, and Gregory Tesz for technical assistance and Cecile Vernochet for critical reading of the manuscript.

References

1. Hussain, M. M. (2014) Intestinal lipid absorption and lipoprotein formation. *Curr. Opin. Lipidol.* **25,** 200–206
2. Kennedy, E. P., and Weiss, S. B. (1956) The function of cytidine coenzymes in the biosynthesis of phospholipides. *J. Biol. Chem.* **222,** 193–214
3. Kern, F., Jr., and Borgström, B. (1965) Quantitative study of the pathways of triglyceride synthesis by hamster intestinal mucosa. *Biochim. Biophys. Acta* **98,** 520–531
4. Johnston, J. M., Rao, G. A., and Lowe, P. A. (1967) The separation of the α-glycerophosphate and monoglyceride pathways in the intestinal biosynthesis of triglycerides. *Biochim. Biophys. Acta* **137,** 578–580
5. Clark, B., and Hubscher, G. (1961) Biosynthesis of glycerides in subcellular fractions of intestinal mucosa. *Biochim. Biophys. Acta* **46,** 479–494
6. Clark, B., and Huebscher, G. (1960) Biosynthesis of glycerides in the mucosa of the small intestine. *Nature* **185,** 35–37
7. Kayden, H. J., Senior, J. R., and Mattson, F. H. (1967) The monoglyceride pathway of fat absorption in man. *J. Clin. Invest.* **46,** 1695–1703
8. Yen, C. L., Cheong, M. L., Grueter, C., Zhou, P., Moriwaki, J., Wong, J. S., Hubbard, B., Marmor, S., and Farese, R. V., Jr. (2009) Deficiency of the intestinal enzyme acyl CoA:monoacylglycerol acyltransferase-2 protects mice from metabolic disorders induced by high-fat feeding. *Nat. Med.* **15,** 442–446
9. Cheng, D., Nelson, T. C., Chen, J., Walker, S. G., Wardwell-Swanson, J., Meegalla, R., Taub, R., Billheimer, J. T., Ramaker, M., and Feder, J. N. (2003) Identification of acyl coenzyme A:monoacylglycerol acyltransferase 3, an intestinal specific enzyme implicated in dietary fat absorption. *J. Biol. Chem.* **278,** 13611–13614
10. Gao, Y., Nelson, D. W., Banh, T., Yen, M. I., and Yen, C. L. (2013) Intestine-specific expression of MOGAT2 partially restores metabolic efficiency in Mogat2-deficient mice. *J. Lipid Res.* **54,** 1644–1652
11. Nelson, D. W., Gao, Y., Yen, M. I., and Yen, C. L. (2014) Intestine-specific deletion of acyl-CoA:monoacylglycerol acyltransferase (MGAT) 2 protects mice from diet-induced obesity and glucose intolerance. *J. Biol. Chem.* **289,** 17338–17349
12. Wendel, A. A., Lewin, T. M., and Coleman, R. A. (2009) Glycerol-3-phosphate acyltransferases: rate limiting enzymes of triacylglycerol biosynthesis. *Biochim. Biophys. Acta* **1791,** 501–506
13. Lewin, T. M., Wang, S., Nagle, C. A., Van Horn, C. G., and Coleman, R. A. (2005) Mitochondrial glycerol-3-phosphate acyltransferase-1 directs the metabolic fate of exogenous fatty acids in hepatocytes. *Am. J. Physiol. Endocrinol. Metab.* **288,** E835–E844
14. Lewin, T. M., de Jong, H., Schwerbrock, N. J., Hammond, L. E., Watkins, S. M., Combs, T. P., and Coleman, R. A. (2008) Mice deficient in mitochondrial glycerol-3-phosphate acyltransferase-1 have diminished myocardial triacylglycerol accumulation during lipogenic diet and altered phospholipid fatty acid composition. *Biochim. Biophys. Acta* **1781,** 352–358
15. Wang, S., Lee, D. P., Gong, N., Schwerbrock, N. M., Mashek, D. G., Gonzalez-Baró, M. R., Stapleton, C., Li, L. O., Lewin, T. M., and Coleman, R. A. (2007) Cloning and functional characterization of a novel mitochondrial *N*-ethylmaleimide-sensitive glycerol-3-phosphate acyltransferase (GPAT2). *Arch. Biochem. Biophys.* **465,** 347–358
16. Nagle, C. A., Vergnes, L., Dejong, H., Wang, S., Lewin, T. M., Reue, K., and Coleman, R. A. (2008) Identification of a novel sn-glycerol-3-phosphate acyltransferase isoform, GPAT4, as the enzyme deficient in Agpat6$^{-/-}$ mice. *J. Lipid Res.* **49,** 823–831
17. Cao, J., Li, J. L., Li, D., Tobin, J. F., and Gimeno, R. E. (2006) Molecular identification of microsomal acyl-CoA:glycerol-3-phosphate acyltransferase, a key enzyme in de novo triacylglycerol synthesis. *Proc. Natl. Acad. Sci. U.S.A.* **103,** 19695–19700
18. Cao, J., Perez, S., Goodwin, B., Lin, Q., Peng, H., Qadri, A., Zhou, Y., Clark, R. W., Perreault, M., Tobin, J. F., and Gimeno, R. E. (2014) Mice deleted for GPAT3 have reduced GPAT activity in white adipose tissue and altered energy and cholesterol homeostasis in diet-induced obesity. *Am. J. Physiol. Endocrinol. Metab.* **306,** E1176–E1187
19. Millar, J. S., Cromley, D. A., McCoy, M. G., Rader, D. J., and Billheimer, J. T. (2005) Determining hepatic triglyceride production in mice: comparison of poloxamer 407 with Triton WR-1339. *J. Lipid Res.* **46,** 2023–2028
20. Desai, U., Lee, E. C., Chung, K., Gao, C., Gay, J., Key, B., Hansen, G., Machajewski, D., Platt, K. A., Sands, A. T., Schneider, M., Van Sligtenhorst, I., Suwanichkul, A., Vogel, P., Wilganowski, N., Wingert, J., Zam-

browicz, B. P., Landes, G., and Powell, D. R. (2007) Lipid-lowering effects of anti-angiopoietin-like 4 antibody recapitulate the lipid phenotype found in angiopoietin-like 4 knockout mice. *Proc. Natl. Acad. Sci. U.S.A.* **104,** 11766–11771
21. Xu, J., Donepudi, A. C., Moscovitz, J. E., and Slitt, A. L. (2013) Keap1-knockdown decreases fasting-induced fatty liver via altered lipid metabolism and decreased fatty acid mobilization from adipose tissue. *PLoS ONE* **8,** e79841
22. Wang, H., Gilham, D., and Lehner, R. (2007) Proteomic and lipid characterization of apolipoprotein B-free luminal lipid droplets from mouse liver microsomes: implications for very low density lipoprotein assembly. *J. Biol. Chem.* **282,** 33218–33226
23. Yet, S. F., Lee, S., Hahm, Y. T., and Sul, H. S. (1993) Expression and identification of p90 as the murine mitochondrial glycerol-3-phosphate acyltransferase. *Biochemistry* **32,** 9486–9491
24. Hall, A. M., Kou, K., Chen, Z., Pietka, T. A., Kumar, M., Korenblat, K. M., Lee, K., Ahn, K., Fabbrini, E., Klein, S., Goodwin, B., and Finck, B. N. (2012) Evidence for regulated monoacylglycerol acyltransferase expression and activity in human liver. *J. Lipid Res.* **53,** 990–999
25. Cartwright, I. J., and Higgins, J. A. (1999) Isolated rabbit enterocytes as a model cell system for investigations of chylomicron assembly and secretion. *J. Lipid Res.* **40,** 1357–1365
26. Iqbal, J., Anwar, K., and Hussain, M. M. (2003) Multiple, independently regulated pathways of cholesterol transport across the intestinal epithelial cells. *J. Biol. Chem.* **278,** 31610–31620
27. Anwar, K., Iqbal, J., and Hussain, M. M. (2007) Mechanisms involved in vitamin E transport by primary enterocytes and in vivo absorption. *J. Lipid Res.* **48,** 2028–2038
28. Shan, D., Li, J. L., Wu, L., Li, D., Hurov, J., Tobin, J. F., Gimeno, R. E., and Cao, J. (2010) GPAT3 and GPAT4 are regulated by insulin-stimulated phosphorylation and play distinct roles in adipogenesis. *J. Lipid Res.* **51,** 1971–1981
29. Ma, S., Jing, F., Xu, C., Zhou, L., Song, Y., Yu, C., Jiang, D., Gao, L., Li, Y., Guan, Q., and Zhao, J. (2015) Thyrotropin and obesity: increased adipose triglyceride content through glycerol-3-phosphate acyltransferase 3. *Sci. Rep.* **5,** 7633
30. Zhu, J., Lee, B., Buhman, K. K., and Cheng, J. X. (2009) A dynamic, cytoplasmic triacylglycerol pool in enterocytes revealed by ex vivo and in vivo coherent anti-Stokes Raman scattering imaging. *J. Lipid Res.* **50,** 1080–1089
31. Lee, B., Zhu, J., Wolins, N. E., Cheng, J. X., and Buhman, K. K. (2009) Differential association of adipophilin and TIP47 proteins with cytoplasmic lipid droplets in mouse enterocytes during dietary fat absorption. *Biochim. Biophys. Acta* **1791,** 1173–1180
32. Buhman, K. K., Smith, S. J., Stone, S. J., Repa, J. J., Wong, J. S., Knapp, F. F., Jr., Burri, B. J., Hamilton, R. L., Abumrad, N. A., and Farese, R. V., Jr. (2002) DGAT1 is not essential for intestinal triacylglycerol absorption or chylomicron synthesis. *J. Biol. Chem.* **277,** 25474–25479
33. Green, P. H., Glickman, R. M., Riley, J. W., and Quinet, E. (1980) Human apolipoprotein A-IV: intestinal origin and distribution in plasma. *J. Clin. Invest.* **65,** 911–919
34. Kohan, A. B., Wang, F., Li, X., Vandersall, A. E., Huesman, S., Xu, M., Yang, Q., Lou, D., and Tso, P. (2013) Is apolipoprotein A-IV rate limiting in the intestinal transport and absorption of triglyceride? *Am. J. Physiol. Gastrointest. Liver Physiol.* **304,** G1128–G1135
35. Kieffer, T. J. (2003) GIP or not GIP? That is the question. *Trends Pharmacol. Sci.* **24,** 110–112
36. Wilfling, F., Wang, H., Haas, J. T., Krahmer, N., Gould, T. J., Uchida, A., Cheng, J. X., Graham, M., Christiano, R., Fröhlich, F., Liu, X., Buhman, K. K., Coleman, R. A., Bewersdorf, J., Farese, R. V., Jr., and Walther, T. C. (2013) Triacylglycerol synthesis enzymes mediate lipid droplet growth by relocalizing from the ER to lipid droplets. *Dev. Cell* **24,** 384–399
37. Smith, S. J., Cases, S., Jensen, D. R., Chen, H. C., Sande, E., Tow, B., Sanan, D. A., Raber, J., Eckel, R. H., and Farese, R. V., Jr. (2000) Obesity resistance and multiple mechanisms of triglyceride synthesis in mice lacking Dgat. *Nat. Genet.* **25,** 87–90
38. Liu, J., Gorski, J. N., Gold, S. J., Chen, D., Chen, S., Forrest, G., Itoh, Y., Marsh, D. J., McLaren, D. G., Shen, Z., Sonatore, L., Carballo-Jane, E., Craw, S., Guan, X., Karanam, B., Sakaki, J., Szeto, D., Tong, X., Xiao, J., Yoshimoto, R., Yu, H., Roddy, T. P., Balkovec, J., and Pinto, S. (2013) Pharmacological inhibition of diacylglycerol acyltransferase 1 reduces body weight and modulates gut peptide release: potential insight into mechanism of action. *Obesity* **21,** 1406–1415
39. Cao, J., Zhou, Y., Peng, H., Huang, X., Stahler, S., Suri, V., Qadri, A., Gareski, T., Jones, J., Hahm, S., Perreault, M., McKew, J., Shi, M., Xu, X., Tobin, J. F., and Gimeno, R. E. (2011) Targeting Acyl-CoA:diacylglycerol acyltransferase 1 (DGAT1) with small molecule inhibitors for the treatment of metabolic diseases. *J. Biol. Chem.* **286,** 41838–41851
40. Villanueva, C. J., Monetti, M., Shih, M., Zhou, P., Watkins, S. M., Bhanot, S., and Farese, R. V., Jr. (2009) Specific role for acyl CoA:diacylglycerol acyltransferase 1 (Dgat1) in hepatic steatosis due to exogenous fatty acids. *Hepatology* **50,** 434–442
41. Lin, H. V., Chen, D., Shen, Z., Zhu, L., Ouyang, X., Vongs, A., Kan, Y., Levorse, J. M., Kowalik, E. J., Jr., Szeto, D. M., Yao, X., Xiao, J., Chen, S., Liu, J., Garcia-Calvo, M., Shin, M. K., and Pinto, S. (2013) Diacylglycerol acyltransferase-1 (DGAT1) inhibition perturbs postprandial gut hormone release. *PLoS ONE* **8,** e54480
42. Miyawaki, K., Yamada, Y., Ban, N., Ihara, Y., Tsukiyama, K., Zhou, H., Fujimoto, S., Oku, A., Tsuda, K., Toyokuni, S., Hiai, H., Mizunoya, W., Fushiki, T., Holst, J. J., Makino, M., Tashita, A., Kobara, Y., Tsubamoto, Y., Jinnouchi, T., Jomori, T., and Seino, Y. (2002) Inhibition of gastric inhibitory polypeptide signaling prevents obesity. *Nat. Med.* **8,** 738–742
43. Maciejewski, B. S., LaPerle, J. L., Chen, D., Ghosh, A., Zavadoski, W. J., McDonald, T. S., Manion, T. B., Mather, D., Patterson, T. A., Hanna, M., Watkins, S., Gibbs, E. M., Calle, R. A., and Steppan, C. M. (2013) Pharmacological inhibition to examine the role of DGAT1 in dietary lipid absorption in rodents and humans. *Am. J. Physiol. Gastrointest. Liver Physiol.* **304,** G958–G969